

Water-Stable Plasma-Polymerized *N,N*-Dimethylacrylamide Coatings to Control Cellular Adhesion

Tim Egghe,^{†,‡} Pieter Cools,[†] Joachim F. R. Van Guyse,[‡] Mahtab Asadian,[†] Dmitry Khalenkov,[§] Anton Nikiforov,[†] Heidi Declercq,^{||} Andre G. Skirtach,[§] Rino Morent,[†] Richard Hoogenboom,^{*,‡} and Nathalie De Geyter^{*,†}

[†]Research Unit Plasma Technology (RUPT), Department of Applied Physics, Faculty of Engineering and Architecture, Ghent University, Sint-Pietersnieuwstraat 41 B4, 9000 Ghent, Belgium

[‡]Supramolecular Chemistry Group, Centre of Macromolecular Chemistry (CMaC) Department of Organic and Macromolecular Chemistry, Faculty of Sciences, Ghent University, Krijgslaan 281 S4, 9000 Ghent, Belgium

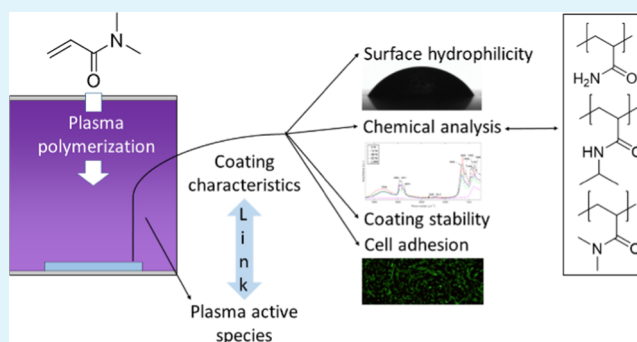
[§]Department of Biotechnology, Faculty of Bioscience Engineering, Ghent University, Coupure Links 653 B, 9000 Ghent, Belgium

^{||}Tissue Engineering Group, Department of Human Structure and Repair, Faculty of Medicine and Health Sciences, Ghent University, Corneel Heymanslaan 10 B3, 9000 Ghent, Belgium

S Supporting Information

ABSTRACT: The plasma polymerization of amide-based precursors is a nearly unexplored research area, which is in contrast with the abundance of reports focusing on amide-based surface modification using wet chemistry. Therefore, this study aims to profoundly investigate the near-atmospheric pressure plasma polymerization of *N,N*-dimethylacrylamide (DMAM) to obtain stable coatings. In contrast to the unstable coatings obtained at lower discharge powers, the stable coatings that were obtained at higher powers showed a lower hydrophilicity as assessed by water contact angle (WCA). This decrease in hydrophilicity with increasing plasma power was found to be related to a reduced preservation of the monomer structure, as observed by Fourier transform infrared (FTIR), Raman spectroscopy, X-ray photoelectron spectroscopy (XPS), and XPS C₆₀ depth profiling, a rarely used but effective combination of techniques. Furthermore, the chemical composition of the coating was found to be in good agreement with the plasma active species observed by optical emission spectroscopy. Additionally, XPS C₆₀ depth profiling indicated a difference between the top layer and bulk of the plasma polymer due to spontaneous oxidation and/or postplasma coating deposition. Finally, the stable coatings were also found to have cell-interactive behavior toward MC3T3 as studied by in vitro live/dead fluorescence imaging and (3-(4,5-dimethylthiazol-2-yl)-5-(3-carboxymethoxyphenyl)-2-(4-sulfophenyl)-2H-tetrazolium) (MTS) assays. With the latter technique, a cell viability of up to 89% as compared with tissue culture plates after 1 day of cell culture was observed, indicating the potential of these coatings for tissue engineering purposes.

KEYWORDS: plasma polymerization, *N,N*-dimethylacrylamide, dielectric barrier discharge, cell-interactive coatings, tissue engineering, surface analysis



1. INTRODUCTION

Nonthermal plasma polymerization has become a popular technology for the deposition of sub-micrometer films. It presents an attractive alternative to more traditional coating procedures via wet chemistry, since it is a simple, one-step, cost-effective, and environmentally friendly technique.^{1,2} Moreover, the coating characteristics can be varied by the selection of the precursor (monomer). One disadvantage, however, is that due to the complex nature of the plasma process, the coating chemistry is hard to predict based on the chemical structure of the precursor. Therefore, extensive surface characterization is required to elucidate the surface properties and chemistry of the resulting plasma-polymerized

coatings and to correlate these to the applied parameters in the plasma process. Over the years, the plasma polymerization process of a wide range of precursors has been extensively studied, including carboxylic acids, alcohols, amines, siloxanes, and ethers.^{3–10} In contrast to these types of monomers, the use of amide-based precursors for plasma deposition has only been reported in a few studies.^{11–15} Pan et al. and Chu et al. reported the plasma-assisted synthesis of thermosensitive films based on, respectively, *N*-isopropylacrylamide (NIPAM) and

Received: October 29, 2019

Accepted: December 13, 2019

Published: December 13, 2019

N,N-diethylacrylamide (DEAM).^{12,14,15} Cheng et al. reported temperature-dependent protein adsorption on plasma coatings based on NIPAM, and Griesser et al. observed good cell attachment and growth on films fabricated by plasma polymerization of *N,N*-dimethylformamide (DMF), *N,N*-dimethylacetamide (DMA), and *N,N*-dimethylpropionamide (DMP).^{11,13}

This relatively small number of reported studies is in contrast with the widespread use of polyamide-based surface modification using wet chemistry.^{16–18} The interest in polyamide-coated substrates is mainly biomedical and is inspired by the large hydrophilicity of these materials that also resemble the chemical structure of proteins and peptides. Surface modification with polymers comprising primary, secondary, and tertiary amides in their repeating unit has been reported for various applications. Among others, polyamides have been employed as antifouling coatings^{19–21} and as carriers for RGD-peptide moieties to make surfaces cell-adhesive.²² Moreover, polyamides can be used to fabricate thermoresponsive surfaces, which are useful for applications like drug delivery and cell patterning and culturing.¹⁷ The broad scope and application potential of polyamide-coated surfaces indicate that plasma polymerization of amide precursors still has an unexplored potential. However, in the few previous reports on plasma deposition of amide precursors, the chemical analysis consisted of only two different techniques and the coating stability study was only limited to 3 h of water incubation. Therefore, a more extensive chemical analysis and stability study of such amide-based coatings are still lacking. The former analysis is needed to understand which functional groups are present in the coating because of the plasma fragmentation processes, as these groups can influence the properties of the coating. The latter study is important as the stability of a plasma-polymerized coating is a critical factor for its application potential as these coatings tend to suffer from poor stability due to insufficient cross-linking during the plasma polymerization process. Stability can be improved by applying higher powers during plasma polymerization, which most often leads to more extensive functional group fragmentation.²³

In this paper, the influence of power on the plasma polymerization of *N,N*-dimethylacrylamide (DMAM) is examined. To the best of the authors' knowledge, DMAM has never been reported before as a monomer in plasma polymerization. This is rather surprising as it seems to be ideally suited for the preparation of amide-based coatings due to its unsaturated nature and lower amount of carbon atoms in the structure compared with the previously studied NIPAM and DEAM, which could, respectively, improve functionality retention and the antifouling capacity of the resulting coating.^{24,25} Moreover, this monomer is relatively inexpensive. A medium-pressure parallel-plate dielectric barrier discharge (DBD) setup was used to deposit DMAM-based coatings on glass substrates, after which the stability, chemical composition, wettability of the coatings, and the optical emission of the plasma were assessed. The coating stability was studied after 1 and 7 days of water incubation, which gives a representative image of long-term stability, as the first 24 h are the most critical for the stability process.²⁶ The chemical analysis was done with Fourier transform infrared (FTIR) spectroscopy, X-ray photoelectron spectroscopy (XPS), XPS C₆₀ depth profiling, and Raman spectroscopy, which is an extension of the standard analysis of plasma polymers that mostly consist of

the first two mentioned techniques.²⁷ This combination of techniques is very interesting, as FTIR and Raman spectroscopy are complementary and XPS depth profiling enables a better comparison with the two previous techniques.²⁸ Namely, FTIR and Raman spectroscopies have a larger analysis depth than XPS, so XPS depth-profiling results are more reliable for comparison with these two techniques. To study the plasma process itself, optical emission spectroscopy (OES) was performed and the plasma active species were linked to the chemical analysis. Glass was chosen as a substrate because of easy handling, the possibility of thickness measurements with scratch tests, and easy substrate distinction in XPS (depth profiling).

Finally, cell adhesion and viability were evaluated for stable coatings by live/dead fluorescence imaging and (3-(4,5-dimethylthiazol-2-yl)-5-(3-carboxymethoxyphenyl)-2-(4-sulphophenyl)-2*H*-tetrazolium) (MTS) assays with osteoblasts from mouse calvaria (MC3T3). These cell tests were performed to evaluate whether the plasma-polymerized coatings can maintain the antifouling properties as shown by poly(*N,N*-dimethylacrylamide) and other tertiary amide-based polymers or whether cell-interactive coatings were obtained as observed by previous studies on related plasma-polymerized coatings.^{13,19–21,25,29,30}

2. MATERIALS AND METHOD

2.1. Materials. All high-performance liquid chromatograph (HPLC)-grade solvents were purchased from either Merck (toluene, hexane, tetrahydrofuran (THF), dichloromethane (DCM)) or Honeywell (diethylether (DEE)). Dry DMF was obtained from a custom-made JW Meyer solvent purification system and was dried over aluminum oxide columns. The following chemicals were used as received unless otherwise stated: polyacrylamide (PACAm) (Acros Organics), chloroform-*d* (CDCl₃, ≥99.8%, Euriso-Top), dimethylsulfoxide-*d*₆ (DMSO-*d*₆, ≥99.9%, Euriso-Top), and DMA (Merck). DMAM (99%, Sigma-Aldrich) was purified by passing over a basic aluminum oxide column to remove the inhibitor. NIPAM (>98%, Scientific Polymer Products Inc.) and 2,2-azobisisobutyronitrile (AIBN) (Sigma-Aldrich, 98%) were recrystallized twice in hexane and methanol, respectively, and subsequently dried in vacuo prior to use. Deionized water with a resistivity ≤1 μS/cm³ was obtained by using a Eurowater filtration device. Argon (Ar) (Alphagaz 1) was purchased from Air Liquide and used as supplied. Large glass coverslips (diameter: 18 mm; thickness: 0.13–0.16 mm) and small glass coverslips (diameter: 12 mm; thickness: 0.13–0.16 mm) were purchased from VWR and used as supplied. Square quartz coverslips (22 mm × 22 mm × 0.25 mm) were purchased from Ted Pella Inc. and used as supplied.

2.2. Reference Polymer Synthesis. To compare the plasma-polymerized coatings with amide-based polymers, poly(*N,N*-dimethylacrylamide) (PDMA) and poly(*N*-isopropylacrylamide) (PNIPAM) were synthesized by free radical polymerization as will be described in this section. Analysis of the synthesis was performed by gas chromatography (GC), ¹H nuclear magnetic resonance (¹H NMR) spectroscopy, and size exclusion chromatography (SEC).

2.2.1. GC. For PDMA synthesis, samples were taken during the polymerization and measured with GC to determine the monomer conversion from the ratio of the integrals of the peaks from the monomer and the reaction solvent. GC was performed on an Agilent 7890A system equipped with a VWR Carrier-160 hydrogen generator and an Agilent HP-5 column of 30 m length and 0.320 mm diameter. A flame ionization detector was used, and the inlet was set to 250 °C with a split injection of ratio 25:1. Hydrogen was used as the carrier gas at a flow rate of 2 mL/min. The oven temperature was increased at 20 °C/min from 50 to 120 °C, followed by a ramp of 50 °C/min to 300 °C.

Table 1. FWHM and Peak Location Constraints for the Fitting Procedure (All Values in eV)

	C 1s		O 1s		N 1s	
	peak location	FWHM	peak location	FWHM	peak location	FWHM
peak 1	284.9–285.1	1.3–1.6	531–531.5	1.4–1.7	399.7–399.8	1.8–1.9
peak 2	285.8–286.2	1.25–1.65	532.25–532.6	1.4–1.7	398.9–399.0	1.8–1.9
peak 3	287.4–288	1.3–2.0	533.6–533.8	1.4–1.7		

2.2.2. ¹H NMR Spectroscopy. ¹H NMR spectra were recorded on a Bruker Avance 300 or 400 MHz spectrometer at room temperature. The chemical shifts are given in parts per million (δ) relative to tetramethylsilane.

2.2.3. SEC. SEC was performed on an Agilent 1260-series HPLC system equipped with a 1260 online degasser, a 1260 ISO-pump, a 1260 automatic liquid sampler (ALS), a thermostatted column compartment (TCC) set at 50 °C equipped with two PLgel 5 μ m mixed-D columns and a precolumn in series, a 1260 diode array detector (DAD), and a 1260 refractive index (RI) detector. The used eluent was DMA containing 50 mM of LiCl at a flow rate of 1 mL/min. The spectra were analyzed using Agilent Chemstation software with the gel permeation chromatography add-on. Molar mass values and \bar{D} values were calculated against poly(methyl methacrylate) standards from Polymer Standards Service.

2.2.4. PDMA Synthesis. For PDMA, DMAM (10.9 g, 0.101 mol) and AIBN (0.0137 g, 0.0834 mmol) were dissolved in toluene (30 mL) in a 50 mL round-bottom flask. Subsequently, the flask was capped with a septum and the polymerization mixture was purged with Ar for 30 min before the vial was placed in a preheated block at 70 °C. The reaction was quenched after 60 min by exposing to air and subsequent cooling. The polymerization had reached 80% conversion, as determined by GC. The product was purified by precipitation into hexane, first from toluene, before being dissolved in THF and precipitated twice more in hexane, after which the polymer was dried in a vacuum oven at 50 °C. ¹H NMR (300 MHz, CDCl₃): δ 3.26–2.54 (m, 6H), 1.92 (s, 1H), 1.85–0.99 (m, 2H). SEC: M_n = 76.7 kDa; \bar{D} = 3.8. The detailed results of the analysis can be found in the Supporting Information (Section 1).

2.2.5. PNIPAM Synthesis. PNIPAM was synthesized through free radical polymerization. NIPAM (56.61 g, 0.5 mol) was dissolved in 100 mL of dry DMF, after which AIBN (0.41 g, 2.5 mmol) was added as the initiator. The solution was purged with nitrogen and heated to 70 °C for 5 h to reach full conversion. After polymerization, the solvent was evaporated and the polymer was separated from the polymerization mixture by precipitation from DCM in a tenfold excess of DEE at 0 °C, after which the polymer was dried in a vacuum oven at 50 °C for several hours and a white powder was obtained. ¹H NMR (400 MHz, DMSO): δ 3.45 (d, 1H), 1.75 (s, 1H), 1.17 (dd, 2H), 0.84 (d, 6H). SEC: M_n = 36.2 kDa; \bar{D} = 2.7. The detailed results of the analysis can be found in the Supporting Information (Section 1).

2.3. Plasma Reactor Setup. The plasma activation and polymerization experiments were performed in a DBD reactor, similar to what has been described in an earlier work.³¹ In short, the cylindrical plasma reactor consisted of two parallel electrodes placed 8 mm away from each other. The lower copper electrode was covered with a ceramic alumina layer, and the upper electrode was a woven stainless steel mesh electrode through which the gas was fed. The lower electrode was connected to a 50 kHz AC power source, and the upper electrode was connected to the ground through a 50 Ω resistor. The composition of the discharge mixture consisting of the monomer DMAM and the carrier gas Ar was controlled via a CORI-FLOW liquid mass flow controller and an El-Flow gas mass flow controller (Bronkhorst), respectively. Before the gas entered the plasma reactor through the upper electrode, it first passed through a glass wool filler to distribute the gas flow more evenly before entering the plasma discharge region. The bottom of the plasma reactor was connected to a simple pumping unit, allowing the evacuation of the plasma reactor and subsequent filling with a reproducible atmosphere.

After application of the glass substrate on the lower electrode, the reactor was pumped down to <0.05 kPa and subsequently flushed with Ar at 3000 standard cubic centimeters per minute (sccm) for 3 min at a pressure of 50 kPa. This purging step was performed to obtain a reproducible gas composition in the plasma reactor. Next, a plasma preactivation step was carried out at 5 kPa (Ar flow of 1000 sccm) for 30 s at a power of 4.3 W to introduce radicals on the glass surface. These can serve as anchor points to improve the covalent bonding of the first coating layer to the glass substrate. Plasma polymerization was then performed immediately after plasma preactivation without exposing the substrates to ambient air. To do so, an Ar flow of 3000 sccm and a monomer flow of 0.2 g/h were used. The system pressure was set to 50 kPa, and the gas discharge mixture flowed for 2 min before applying the power to obtain a more reproducible equilibrium between inflow and outflow of the gas. The treatment time was varied between 1 and 10 min, and the applied power varied between 5 and 50 W.

To electrically characterize the DBD, the applied high voltage and the resultant discharge current were measured. The high voltage applied to the lower copper electrode was measured using a 1000:1 high-voltage probe (Tektronix P6015A). The discharge current was obtained by measuring the voltage across a 50 Ω resistor connected in series with the reactor to the ground. Via Ohm's law, the discharge current was calculated. The obtained waveforms were recorded using a digital oscilloscope (Picoscope 3204A), and the discharge power was calculated by performing a discrete integration method of the multiplication of voltage and current, which has been described in a previous work.³¹

2.4. Static Water Contact Angle (WCA) Analysis. WCA measurements were performed at room temperature, using a commercial Krüss Easy Drop system (Krüss GmbH, Germany). Per sample, four (at low WCA) to seven (at high WCA) water droplets of 2.0 μ L of deionized water were placed on different positions of the sample surface. Measurements were performed in triplicate on samples obtained in different plasma experiments. WCAs were measured within 5 min after the coating deposition.

2.5. XPS and XPS Depth Profiling. XPS surface analysis was performed on a PHI 5000 Versaprobe II spectrometer. This equipment used a monochromatic Al K α X-ray source ($h\nu$ = 1486.6 eV) operating at 23.5 W. A vacuum of at least 10⁻⁶ Pa was obtained for all measurements. Survey scans and high-resolution spectra (C 1s, N 1s, and O 1s) were recorded with pass energies of 187.85 eV (eV step = 0.8 eV) and 23.5 eV (eV step = 0.1 eV), respectively, at an angle of 45° to the normal of the sample and a spot diameter of 50 μ m. Four points per sample were measured. Multipak (v9.6.1) was used for elemental analysis using a Shirley background, and the relative sensitivity factors were supplied by the manufacturer. Fitting of the high-resolution peaks was also performed by using Multipak after applying a Savitzky–Golay smoothing procedure. Therefore, the spectra were calibrated at 285.0 eV (C–C bond) prior to analysis. The peaks were deconvoluted by using Gaussian–Lorentzian peak shapes. The full width at half-maximum (FWHM) and peak location constraints are shown in Table 1. An example of the applied fitting is given in Figure 1. The fitting is only used for the quantification of amides and C=O groups, as these are the only groups that can be clearly separated from other chemical functionalities and are the most relevant for the coating analysis. Therefore, the energies in the C 1s spectrum corresponding to C–C, C–H, C–N, C–O, C=N, and C≡N are not fitted by separate peaks, as they significantly overlap and as the introduction of more peaks would lead to arbitrary quantification of these groups. As such, all of

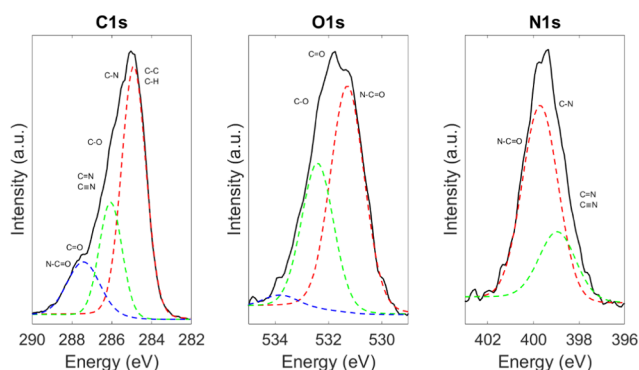


Figure 1. Example of the applied fitting procedure.

these bonds are fitted by two broader peaks, which do not relate to any specific bond, to specifically quantify the part of the C 1s spectrum that relates to C=O groups and amides. As such, the former two peaks are not used for quantification, while the third peak is quantified as this contains the functionalities of interest. For O 1s, the fitting is slightly more arbitrary, but it is possible to make a distinction between amides and C=O groups. Peak 1 is used to describe amides, and the values are based on the XPS spectra of the reference polymers that are described in the Supporting Information in Section 2.3. Peak 2 is composed of both double- and single-bonded oxygen to carbon, as C=O and C–O groups are, respectively, found at 532.2 ± 0.2 and 532.8 ± 0.2 eV.³² It could be possible to fit these functionalities with two different peaks, but this would lead to an arbitrary quantification of the respective chemical groups, while the interest of the fitting is to make a distinction between amides and C=O groups. Peak 3 is needed to obtain a good fit, but it is difficult to assign chemical functionalities in this region. The fit for N 1s is included for clarity reasons but will not be used for quantification as the energies of the different groups are too close to each other to extract any meaningful data.³³

XPS sputter depth profiles were collected with azimuthal Zalar Rotation using a PHI 06-C₆₀ cluster ion gun that was operated at 10 kV and 10 nA and which was raster-scanned over a 4 mm × 4 mm area. Zalar Rotation was achieved by rotating the sample while maintaining the analysis area centered during the sputter cycle. This significantly improved interface layer definition by eliminating sputtering artifacts that may occur when sputtering at a fixed angle. An X-ray setting of 100 μm and 25 W and an analyzer pass energy of 23.5 eV were used for all sputter depth profiles. The atomic contents were plotted as a function of depth, by calibrating the sputter time as a function of the thickness measured with atomic force microscopy (AFM). For all measurements, a deposition time of 2 min was used, which led to a different coating thickness as the deposition rate varies as a function of power. The time needed to sputter the complete coating was determined by picking the first point at which the Si% was >1%.

2.6. FTIR Spectroscopy. A Bruker Tensor 27 spectrometer equipped with a single reflection attenuated total reflectance (ATR) accessory (MIRacle, Pike technology) was used to perform FTIR analysis on coated glass substrates, using a germanium crystal as the internal reflection element. All spectra were recorded using a mercury cadmium telluride (MCT) detector (liquid N₂ cooled) in the spectral region of 4000–700 cm⁻¹, and 64 scans (resolution 4 cm⁻¹) were made for each sample. OPUS 7 software was used to analyze the obtained spectra and to correct for the presence of CO₂ peaks within the spectra, originating from the ambient environment. Two measurement points on three samples per condition were used. The deposition time was 5 min for all conditions.

2.7. Raman Spectroscopy. Raman spectroscopy was performed with a confocal Raman microscope (WITec Alpha300R+) equipped with a UHTS 300 spectrometer, a –70 °C cooled charge-coupled device (CCD) camera (iDus 401 BR-DD, ANDOR), and a 785 nm excitation diode laser (Toptica). A 40×/0.6NA objective (Nikon) was

used. Laser power, measured before the objective, was set to 180 mW, and the integration time was 20 s. Three measurement points on each sample were used. As the deposition rate varies for different powers, the deposition time is adjusted for each condition to obtain a similar coating thickness (± 450 nm) on the quartz substrates. The deposition times were 10, 8, and 6 min for powers of 5, 12, and 50 W, respectively. Quartz was used as substrates to avoid interfering background signals in the wavenumber region of interest. The spectra were normalized on the largest peak between 300 and 500 cm⁻¹, which originated from the quartz. To evaluate the spectra in a quantitative way, integrations of the peaks were performed by a discrete integration method with Matlab (version R2016b). The boundaries of the peaks were 1414–1490 and 2830–3050 cm⁻¹.

2.8. Thickness Measurements and Stability Evaluation. The thickness of the coatings was assessed by making a scratch in the plasma polymer and measuring the step height with AFM. Therefore, images of 45 μm × 5 μm were made with the step in the middle of the long side of the rectangular image, and the thickness was assessed by taking the average difference in height on both sides of the step. All measurements were performed by an XE-70 atomic force microscope (Park Systems), used in the noncontact mode with a silicon cantilever (NanosensorsTM PPP-NCHR). To quantify the stability of the coatings, glass samples were incubated in deionized water for 1 and 7 days at 37 °C, while control samples were stored under vacuum. For each condition, the coating thickness of three samples was measured, with seven measurement points for each sample, randomly distributed over the total sample surface.

2.9. OES. OES analysis of the plasma gas phase was performed by using an optical spectrometer (Ocean Optics, S1000-USB) with a spectral resolution of 0.7 nm in the wavelength range 250–900 nm. To detect the optical emission spectra of the plasma in the DBD, an optical fiber was placed in front of a quartz window mounted on the reactor.

2.10. In Vitro Testing of Cellular Interactions. All samples were first decontaminated by exposure to UV light (254 nm) for 30 min. Mouse calvaria 3T3 (MC3T3) subclone preosteoblast cells (ATCCs) were seeded onto the samples in a 24-well plate at a density of 40,000 cells/1000 μL of medium per well. Cell culturing was performed using α-MEM glutaMAX-1 (Gibco) medium containing 10 vol % fetal bovine serum (FBS heat inactivated) and 1 mM sodium pyruvate (Invitrogen). The cell-seeded samples were subsequently incubated at 37 °C under 5% CO₂ for 1 day. Cell adhesion and viability were examined 1 day after cell seeding by fluorescence imaging (Type U-RFL-T, Olympus, XCellence Pro software) after live/dead staining and by a (3-(4,5-dimethylthiazol-2-yl)-5-(3-carboxymethoxyphenyl)-2-(4-sulphophenyl)-2H-tetrazolium) (MTS) assay, respectively. For live/dead staining, living cells were stained with calcein AM (Anaspec) and dead cells were stained with propidium iodide (Sigma-Aldrich). The cells were subsequently visualized with a fluorescence microscope (Olympus IX 81) making use of appropriate filters. After performing the MTS assay, the absorbance of the formazan dye in the solution was measured with a 490 nm Universal microplate reader (EL 800, BioTek Instruments). For the coatings, samples without cell seeding were subjected to the MTS assay to take the interaction of MTS and the coating into account (negative control). This absorbance was subtracted from the absorbance of coatings with cell seeding, and these results were normalized to the cell metabolic activity measured on tissue culture polystyrene plates (TCPs). For the glass substrates, no negative control is taken into account. For each condition, the average of six independent measurements conducted on six different samples was taken. For the negative control, the average of three independent measurements conducted on three different samples was taken.

3. RESULTS AND DISCUSSION

3.1. Plasma Polymerization of DMAM. In this study, coatings are deposited by the plasma polymerization of DMAM on glass, which was chosen as a substrate because of easy handling, the possibility of thickness measurements with

scratch tests, and easy substrate distinction in XPS (depth profiling). During the plasma polymerization process, a gas mixture of the evaporated monomer and Ar was flowed into the parallel-plate DBD plasma reactor. A continuous power was applied, which varied from 5 to 50 W. Representative waveforms for each power under study are shown in the Supporting Information (Figure S8). The current waveform is a sinusoidal function on which one large broad band and a couple of small broad bands are superimposed. This indicates that the discharge is operating in the pseudo-glow regime, which enables homogeneous plasma treatment.³⁴ By fixing the monomer flow rate at 0.2 g/h, the working pressure at 50 kPa, and the Ar flow rate at 3000 sccm, the influence of the varying power and time on the chemical composition and stability of the obtained coatings was examined. This approach was chosen because previous studies with similar systems indicated that power has a major influence on these coating characteristics.^{23,31}

3.2. Wettability. The influence of the plasma polymerization process was first evaluated by measuring the wettability of the deposited coatings as a function of power and plasma deposition time. Figure 2 shows three clearly distinguishable

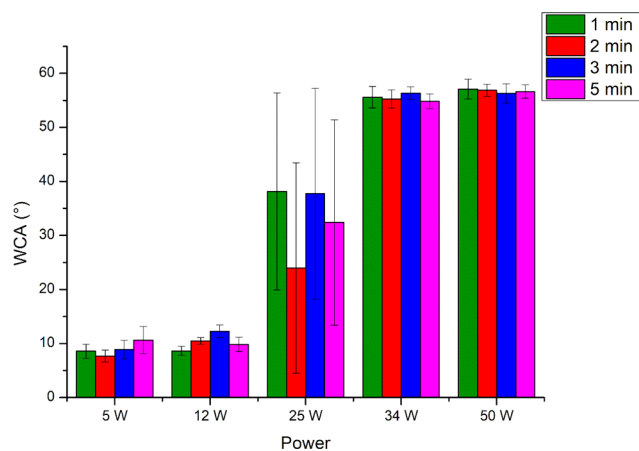


Figure 2. WCA for the plasma polymer as a function of deposition time and power.

regimes for the WCA values. At low powers, the resulting WCAs are low, indicating very hydrophilic coatings. The average WCA over the measurements at 5 and 12 W and the four different time points is $9.6 \pm 1.4^\circ$, showing that the variation between these measurements is small. Therefore, it can be concluded that within this regime (regime I), the deposition time and power have no influence on surface wettability. The second regime occurs at intermediate power (regime II). This regime is characterized by large standard deviations and a large variation in average WCA values as a function of time, with single WCA values varying between 6.9 and 57° and standard deviations as high as 19.5° , indicating that in this regime no homogeneous coatings in terms of wettability could be deposited. The third regime (regime III) occurs at higher powers and is characterized by WCAs that are similar as a function of time and power. The average over all measurements at 34 and 50 W is $56.1 \pm 0.8^\circ$. A closer look at the WCA results in regime II indicates that these WCAs mainly comprise values that occur either in regime I (ranging from 6.9 to 15°) or in regime III (ranging from 49 to 57°). However, some intermediate values also occur. The WCA values in all

three regimes differ from the WCA of the plasma-activated glass substrate ($17.9 \pm 5.2^\circ$; $63.0 \pm 7.3^\circ$ is the WCA prior to activation), indicating that the glass is completely covered by the plasma polymerization process. It should also be noted that 34 W was experimentally found to be the boundary at which regime III starts.

The trend of the WCA values as a function of power shows resemblance with the plasma polymerization of 2-oxazolines, another N- and O-containing monomer.^{31,35,36} Especially the work performed in our group at the same setup shows completely similar results: a regime in which the wettability is high and uniform at low powers, a regime at high powers in which the wettability is lower and constant over a wide range of powers, and an intermediate regime in which the WCAs are not uniform and show resemblance to values of both the first and third regimes. This trend can be caused by local nonuniformities in flow or electrical field in the plasma setup. This is in contrast with other precursors like acrylic acid and allylamine, which show a gradual increase in WCA as a function of power.^{37,38} Furthermore, these results indicate that in regimes I and III, the wettability is the same for the different deposition times. This suggests that the deposition process is time-independent, as observed for other precursors.^{37,39} As the results in regimes I and III are reproducible, in contrast to regime II, the chemical analysis was only performed for these powers.

3.3. Chemical Analysis of the Plasma-Polymerized DMAM Coatings. To evaluate and interpret the FTIR, Raman, and XPS spectra of the DMAM plasma coatings, the respective spectra of three reference polymers were first recorded. Polyamides (PACams) with primary, secondary (PNIPAM), and tertiary amide (PDMA) groups in the repeat unit were chosen as references to assess the differences between the different amides. There are multiple studies about the spectra for these types of polymers, but a comparison between the polymers for all of the different techniques, such as XPS, is currently lacking in the literature. Furthermore, these measurements provide an equipment-specific reference for the evaluation of the plasma polymers. The analysis of the reference polymers is described in Section 2 of the Supporting Information and is used as the basis for the chemical evaluation of the plasma-polymerized DMAM coatings.

3.3.1. FTIR Spectroscopy of the Plasma-Polymerized DMAM Coatings. Figure 3A shows the FTIR spectra of the coatings at regimes I and III. Two spectra were recorded on three different samples for each power for 5 min of deposition, revealing six very similar spectra. Therefore, only one FTIR spectrum is shown for each power under study. The coatings deposited at regime I (5 and 12 W) have similar spectra, while the coatings deposited at regime III (34 and 50 W) also have similar spectra, albeit different from regime I, which indicates a similar chemistry for those coatings obtained within the same regime. The peaks in the region $3000\text{--}2800\text{ cm}^{-1}$ (C–H stretching) and the broad but small peaks located at 2243 and 2180 cm^{-1} that are assigned to $\text{C}\equiv\text{N}$ and $\text{C}\equiv\text{C}$ functionalities are present for all coatings. Additionally, all coatings also show peaks at 1454 , 1379 , and 1344 cm^{-1} , of which the former two could be related to CH_3 deformation, as observed in PNIPAM. The peak at 1344 cm^{-1} could not be observed in the reference polymers, originating possibly from cross-linked C–C bonds.⁴⁰

The FTIR spectra depicted in Figure 3A, however, also show differences between regimes I and III. The broad peak between

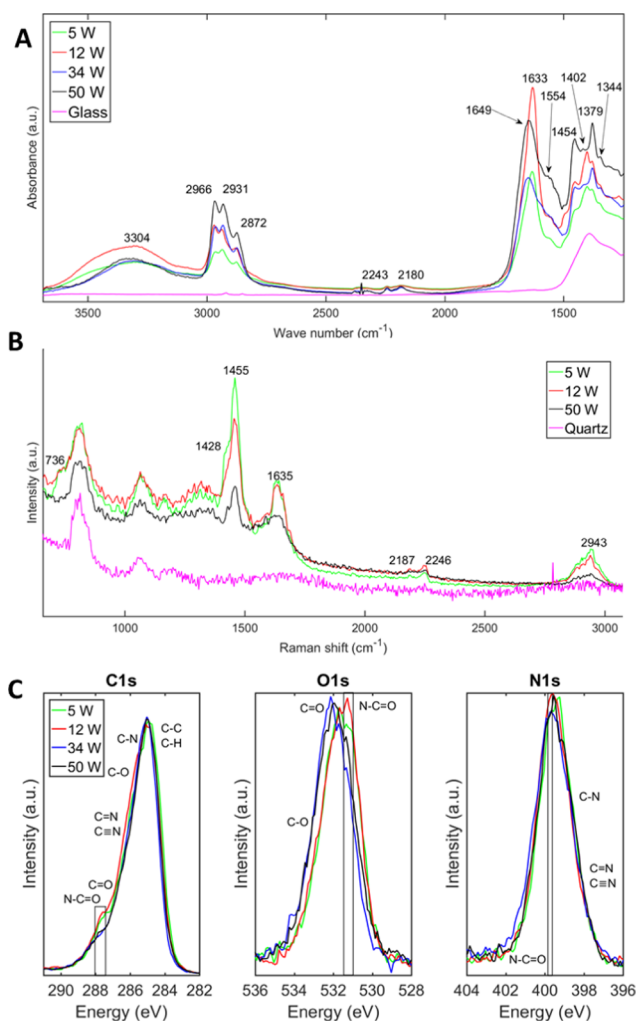


Figure 3. (A) FTIR spectra of the plasma polymers for regime I (5, 12 W) and regime III (34, 50 W), compared with the glass substrate. (B) Raman spectra of the coatings deposited at 5, 12, and 50 W, in comparison with the quartz substrate. (C) High-resolution spectra of the plasma polymers as a function of power for regime I (5, 12 W) and regime III (34, 50 W).

3650 and 3000 cm⁻¹ (N–H or O–H stretching) is narrower for the coatings in regime III. In contrast, the peak between 1750 and 1580 cm⁻¹ (C=O stretch of amides) is broader. By using the reference polymer values of the amide I band, a number of conclusions could be drawn. First, it is clear that the peak location of the amide I band for the coatings at low powers is similar to the peak location of the parent polymer (1635 cm⁻¹), which indicates the presence of a substantial amount of tertiary amides. However, the peak broadening also indicates a more complex chemical environment of the amide bonds and/or the presence of other chemical bonds. These could be primary and/or secondary amides and/or ketones and aldehydes. At higher powers (regime III), the amide I peak shifts to a higher wavenumber, indicating a decrease in tertiary amide content and an increase in the formation of primary/secondary amides and/or ketones/aldehydes. At higher powers, the shoulder of the amide I peak located at 1600 cm⁻¹ and the peak found at 1554 cm⁻¹ (N–H stretch) becomes more pronounced, which is a strong indication for the presence of higher amounts of primary/secondary amides and/or amines. The peak at 1402 cm⁻¹, which most likely arises

from symmetric CH₃ deformation as observed in PDMA, is more pronounced for the coatings in regime I. This indicates that at high powers, the monomer is fragmented to a higher degree. Moreover, the peaks at 2243 and 2180 cm⁻¹ (C≡N and C≡C) are more pronounced for the coatings in regime III. As such, all of these differences in the FTIR spectra could help explain the transition in the coating wettability. Unfortunately, the background spectrum of the glass hindered the analysis of FTIR peaks below 1250 cm⁻¹, but previous studies already showed that these peaks are usually of little added value.^{12,31} The presence of NH and/or OH, C≡N, and/or C≡C and primary/secondary amides indicates that the monomer has been significantly fragmented during the plasma deposition process. The aforementioned chemical groups have also been observed in previously reported FTIR spectra of plasma-polymerized *N,N*-diethylacrylamide,¹² thus confirming the here-described observations.

3.3.2. Raman Spectroscopy of the Plasma-Polymerized DMAM Coatings. Figure 3B shows the Raman spectra of the coatings deposited at 5, 12, and 50 W for similar thicknesses, as obtained by, respectively, depositing for 10, 8, and 6 min. In this particular case, quartz glass is used as a substrate to obtain spectra without interfering background signals in the wavenumber region of interest. WCA measurements on these different substrates indicated similar values for the plasma polymerization experiments at 5, 12, and 50 W in comparison to the WCA values on the glass substrates. For 34 W, the WCA was however not in accordance with the values obtained in regime III, and these spectra were therefore not recorded. For each condition, three Raman spectra were measured, and since these were all similar, only one Raman spectrum is shown to compare the spectra as a function of power (Figure 3B).

The Raman spectra at 5 and 12 W are very similar, as also observed with FTIR spectroscopy, which further confirms the comparable coating chemistry for those deposition parameters falling within regime I. By comparing these spectra with the spectra of bare quartz, the peaks originating from the coating could be distinguished. Similar to the FTIR spectra, the peak at 2943 cm⁻¹ originates from C–H stretching, and the broad low-intensity bands with peaks at 2187 and 2246 cm⁻¹ are observed for all spectra.⁴¹ These bands could again be related to the C≡N and/or C≡C group.⁴⁰ The peak in the region 1428–1455 cm⁻¹ is also present at all powers under investigation. The reference polymers indicated that these CH₂ bending (1455 cm⁻¹) and CH₃ deformation (1428 cm⁻¹) peaks were related to the backbone of the polymer structure. To evaluate the trend as a function of power, the ratio of the integration of the peak at 1428–1455 cm⁻¹ to the other carbon-related peak in the spectra at 2943 cm⁻¹ is compared as a function of power. For 5 W the peak ratio is 2.05 ± 0.06, for 12 W this is 2.14 ± 0.6, and for 50 W the peak ratio is 2.83 ± 0.22. This indicates that the coatings deposited at higher power have a higher expression of the peak at 1428–1455 cm⁻¹, compared with the peak at 2943 cm⁻¹. Additionally, the Raman spectra also show differences between the different deposition regimes. The peak at 736 cm⁻¹ disappears completely for the coating deposited at 50 W, while the peak at 1635 cm⁻¹ is also less pronounced at this high power. These peaks could be related to the diminishing presence of tertiary amides in the coatings at high powers in comparison to the low-power coatings. The band at 736 cm⁻¹ is related to antisymmetric C–N–C stretching in tertiary amides, while the peak at 1635 cm⁻¹ originates from C=O stretching (amide I

band).⁴² The peak location lies in between the peak locations of the amide I band in the tertiary and secondary amide reference polymers. This could be an indication that these types of amides are present at higher concentrations compared with the primary amides. In addition to this qualitative comparison, a quantitative comparison is made by calculating the ratio of the integration of the peak at 1635 cm^{-1} over the carbon-related peak in the spectra at 2943 cm^{-1} as a function of power. This ratio increased from 0.55 ± 0.01 at 5 W to 0.76 ± 0.04 at 12 W and 1.71 ± 0.19 at 50 W. As the amide peak at 736 cm^{-1} is absent, this trend can be an indication of formation of primary or secondary amides at higher powers or of other groups that are Raman-active at this Raman shift, such as imines and/or C=C, which are to be expected at 1690–1640 cm^{-1} and/or 1680–1620 cm^{-1} , respectively.⁴⁰

3.3.3. XPS of the Plasma-Polymerized DMAM Coatings. The XPS results consist of two parts: elemental composition of the coatings based on XPS surveys and chemical group identification by curve fitting high-resolution spectra of the coatings. The elemental composition of the coatings as a function of power is shown in Table 2. The XPS results for the coatings are all for 1 min of plasma polymerization, as the WCA indicated that the process was time-independent.

Table 2. Chemical Composition (in atom %) of the Coatings as a Function of Power

	C %	N %	O %
5 W	73.9 \pm 0.7	14.3 \pm 0.4	11.8 \pm 0.6
12 W	73.3 \pm 1.0	15.1 \pm 0.9	11.6 \pm 0.6
34 W	77.3 \pm 0.8	14.1 \pm 0.6	8.5 \pm 0.3
50 W	76.2 \pm 0.9	14.4 \pm 0.7	9.4 \pm 1.0

As expected, the coating consists of carbon, nitrogen, and oxygen, the three elements that form the monomer. The absence of silicon indicates that the surface is completely covered by the coating after a deposition time of 1 min. The chemical composition of the coatings deposited at 5 and 12 W (regime I) is very similar, as well as the composition of the coatings deposited at 34 and 50 W (regime III). When comparing the low (5 and 12 W) and high (34 and 50 W) powers, the N content is comparable, while the C content and O content are, respectively, higher and lower in regime III. In all cases, the O content is lower than the N content, which was also observed for the aforementioned plasma polymerization of 2-oxazolines.^{31,35,43}

Figure 3C shows the high-resolution C 1s, O 1s, and N 1s spectra for the coatings deposited at different powers. Using all three high-resolution spectra is a new approach as the previous studies on plasma-polymerized amide coatings have only focused on the C 1s spectra.^{11–14} The black boxes indicate the binding energy range corresponding to the amide structure, as derived from the reference polymers (Figure S7). As expected from WCA and XPS survey measurements, the high-resolution

spectra at 5 and 12 W are very similar, as well as the high-resolution spectra at 34 and 50 W, indicating that the chemical composition is comparable within both regimes. In between the two regimes, clear differences could be observed. For the C 1s spectra, the peak corresponding to amides and ketones/aldehydes is more pronounced at low powers. For the O 1s spectra, there is a peak shift toward higher binding energies for the coatings of regime III. The lower peak corresponding to the amide, aldehyde, and ketone groups in the C 1s spectra and the shift in O 1s spectra indicate that higher amounts of amide bonds in the precursor have been fragmented due to the higher power input. This can be concluded because the characteristic O 1s binding energy of amides is lower than the energy of ketones/aldehydes, as discussed in Section 2.3 in the Supporting Information. Furthermore, the width of the O 1s peak suggests that also single-bonded oxygen is present in the coating. Additionally, a third small peak had to be included in the O 1s peak fitting. Normally, this peak corresponds to O=C–O, but as the C 1s spectra do not show this bond, this seems rather unlikely. Possibly, this peak could be attributed to N=C–O or other less electronegative oxygen atoms, like indicated for poly(2-isopropenyl-2-oxazoline).³¹ The shift in the O 1s toward higher energies for the coatings of regime III also indicates that C–O bonds will be relatively more prevalent for these conditions. The N 1s spectra also illustrate that certainly not every N atom is incorporated as an amide, suggesting also the presence of amines, imines, and/or (iso)nitriles. As mentioned before, this peak is not used for quantification as the energies of the different groups are too close to each other to extract any meaningful data.³³

To further study the chemical composition of the coating, a fitting procedure as discussed in Section 2.5 was employed to estimate the amount of amides compared to ketones/aldehydes. C 1s and O 1s spectra were fitted, using three peaks for both spectra, while N 1s was not fitted because the energies of the different groups were too close to each other to extract any meaningful data.³³ The results for the amide-related peaks are shown in Table 3. The absolute combined percentage of amide and C=O content and the percentage of amide content could be estimated by using the respective elemental compositions of C and O. It is observed that the percentage of amide and C=O content from C 1s and the percentage of amide from O 1s are correlating better for the low powers than high powers. This indicates that the shoulder peak at the higher binding energy end of the C 1s spectrum could not be solely assigned to amides, confirming that notable amounts of ketones/aldehydes are formed/incorporated at high powers (regime III). For regime I, most of the groups at this energy are amides, which is in line with the expectations based on previous work as well as FTIR and Raman spectroscopic results. However, it should be noted that the values in Table 3 should be considered as a qualitative estimation of the amide to ketone/aldehyde content because of the arbitrary O 1s fitting.

Table 3. Estimation of Amide and Ketone/Aldehyde Content from C 1s and O 1s Fitting

	amide + C=O % in C 1s	estimated amide + C=O % in coating	amide % in O 1s	estimated amide % in coating
5 W	12.8 \pm 1.0	9.5	68.8 \pm 3.5	8.1
12 W	14.1 \pm 1.2	10.0	65.4 \pm 4.4	7.6
34 W	9.1 \pm 0.4	7.0	42.2 \pm 1.7	3.6
50 W	9.3 \pm 0.2	7.0	37.0 \pm 3.1	3.5

These XPS data are in line with the observed trends in the WCA measurements. Within each regime, the latter measurements indicated a similar wettability, while the former illustrated similar atomic composition and high-resolution spectra. In between the regimes, a lower wettability was observed at higher powers. This can be associated with the chemistry change in the top layer, which consists of a difference in O- and C-contents and a change in functional groups present at the surface. The high-resolution peaks clearly indicate a lower presence of amides, which are highly polar groups, at high powers. For the coatings in regime III, the amides get converted to less polar groups like ketones/aldehydes and alcohols or ethers as observed in the O 1s spectra. As such, the difference in atomic composition and the associated change from more polar to less polar functional groups when the power increases is consistent with the WCA measurements. The combination of XPS and WCA measurements also indicates the presence of a critical point at which the plasma power for a certain monomer flow is sufficient to fragment most of the amide functionality of the precursor, leading to lower wettability and large differences in coating composition. This transition is not gradual but happens quite suddenly. As small variations in the mass flow are inevitable, this sudden transition can be an explanation of the nonuniformity in WCA at the intermediate regime: some areas of the sample are already in regime III, with a slightly lower mass flow resulting in high WCAs, while other areas are still in regime I with a higher mass flow resulting in low WCAs. This shows that the reactor geometry plays a crucial role in the deposition of plasma polymer coatings.

3.3.4. XPS Depth Profiling for the Plasma-Polymerized DMAM Coatings. Besides the XPS spectra of the coating's surface, also XPS spectra of the bulk were recorded by using C₆₀ depth profiling. The results are shown in Figure 4A. The standard deviation for the elemental composition in the bulk of the plasma polymers is for all elements and powers <0.7%. This indicates that the elemental composition is homogeneous over the bulk. It is also clear that the chemical composition in the bulk differs from the top layer for both examined powers (12 and 50 W). The N % is comparable throughout the bulk of the coating, but the O % is higher for low and high powers on the top coating surface, while the C % is consequently lower on the top coating surface. The sputter rate also differs between the two conditions: at 12 W, the sputter rate is approximately 21 nm/min, while at 50 W, it is approximately 12 nm/min. This can be an indication of the more cross-linked structure and higher fragmentation of the coatings deposited at higher powers.

Besides the comparison for chemical composition, also the high-resolution C 1s, O 1s, and N 1s spectra of the top and bulk are compared for both powers, and these results are displayed in Figure 4B. The C 1s spectra show that for both powers the top layer has a more pronounced shoulder corresponding to amides + C=O. By performing the fitting for C 1s as explained in Section 2.5, the amide + C=O content for 12 W is 15.2% at the top and 10.9 ± 1.6% in the bulk (mean and standard deviation calculated over all measurement points in the bulk). For 50 W, this content is 9.4% at the top and 5.8 ± 1.3% in the bulk. The O 1s spectra display a shift toward higher binding energies going from the bulk to the top layer, while the N 1s spectra do not show any difference between the bulk and the top layer as a function of power. Combining the results for C 1s and O 1s spectra with

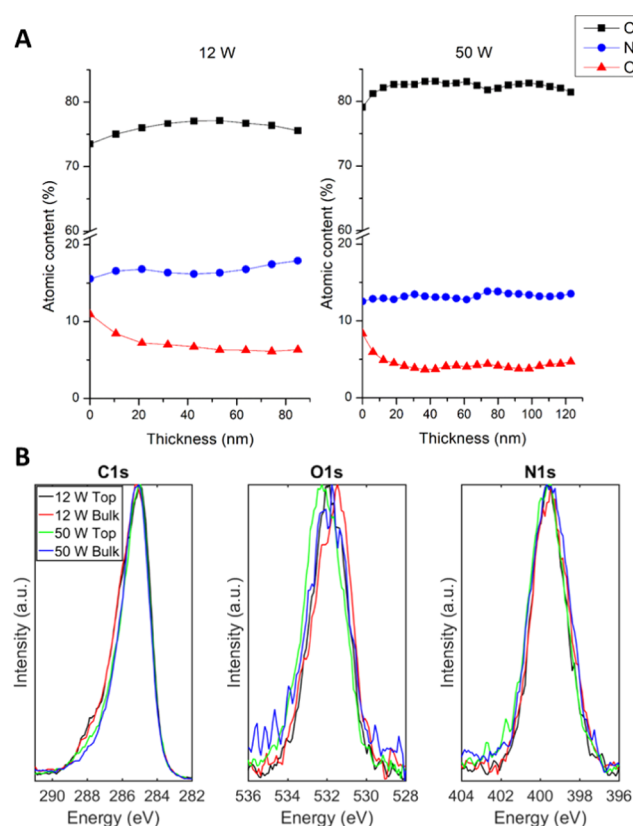


Figure 4. (A) Elemental composition of coatings deposited at 12 and 50 W as a function of coating depth as obtained from C₆₀ depth-profiling measurements. (B) High-resolution spectra of the top layer and bulk of the coating deposited at 12 and 50 W.

the reasoning given in the previous section (shift to higher O 1s binding energies means a lower amide content), it could be concluded that the amide over C=O ratio is higher in the bulk than in the top layer. The formation of C=O in the top layer, and likely also (hydro)peroxides, could result in the observed shift, a phenomenon that has been attributed to the reaction of radicals with air.²⁴ Together with the different C/O ratios on the top and in the bulk, this is a strong indication that there has been a spontaneous reaction between the coating and ambient air. However, also the deposition of a less fragmented top layer, which could be due to postplasma deposition before the reactor is pumped down, could contribute to these results. Both mechanisms have already been proposed by Friedrich.²⁴

Combining XPS and XPS depth-profiling results clarifies the trends in the amide I region for FTIR and Raman spectroscopies. By combining the results from all analytical techniques, it becomes clear that the amide content significantly differs between regimes I and III as defined in Section 3.1. The shift in the amide I peak in FTIR spectroscopy in regime III can at least partially be related to ketone/aldehyde formation in XPS (depth profiling). The higher ratio of the amide I/carbon-related peak in the Raman spectra in regime III cannot be explained by formation of primary or secondary amines, as excluded by XPS (depth profiling). This suggests the presence of unsaturated carbon-carbon bonds and/or imines. An additional proof of the presence of amides in regime I can be found in Figure S9 in the Supplementary Information, in which the NMR spectrum of a dissolved coating is shown and compared to the NMR spectra of DMAM and PDMA. The peak with a chemical shift of 3

ppm that corresponds to methyl hydrogens neighboring the amide nitrogen in PDMA is also observed in the coating, which indicates (partial) preservation of the monomer structure in the dissolved coating.

3.4. Coating Stability. The above chemical analysis illustrated that the coatings of regime II were mainly constituted of a combination of regimes I and III. Therefore, and because of the unreproducible results obtained with WCA, the power in this regime (25 W) is excluded from the coating stability study. Figure 5 shows the results of this study.

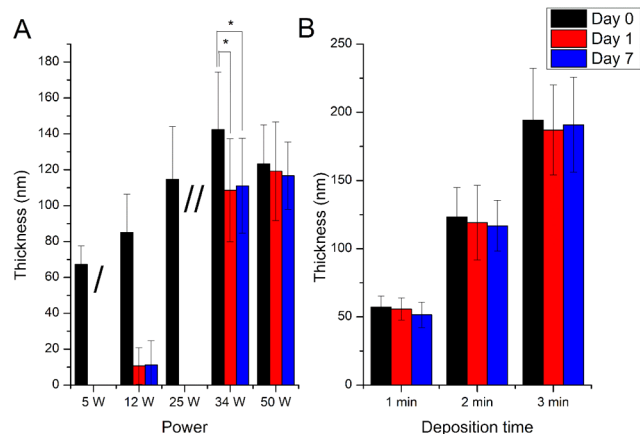


Figure 5. (A) Stability assessment of the coating at different powers for a deposition time of 2 min. (//) Not measured because the coatings were not stable at 5 W. (//) Not measured because of unreproducible WCAs. (*) Are statistically significant differences as calculated with one-way analysis of variance (ANOVA) ($p < 0.05$). (B) Stability assessment of the coating at different deposition times for 50 W incubated for 0, 1, and 7 days in water.

Figure 5A presents the stability study of the plasma-polymerized coatings at different powers for a deposition time of 2 min. At 50 W, the difference in thickness after 1 and 7 days of water incubation is not statistically significant (one-way ANOVA, $p < 0.05$). Therefore, the coating is considered stable at these conditions. At 34 W, the coating thickness significantly decreases after 1 day of water incubation but remains stable afterward as no coating decrease is observed from 1 to 7 days of water incubation (one-way ANOVA, $p < 0.05$). This suggests that an initial unstable layer of the coating is washed away due to the water incubation, but a stable layer underneath remains. This coating could therefore also be considered as stable. Therefore, the coatings deposited at powers higher than 34 W could be considered stable. For the coatings at 12 W, it is observed that nearly all of the coating was removed after 1 day of water incubation. With AFM, it was impossible to observe a scratch on each measurement point for this condition, indicating that most, if not all, of the coating was removed. In that situation, the thickness was defined as 0 nm. As the coatings at 5 W are expected to have even lower stability, these measurements were not performed.⁴⁴ From the measurement at 12 W, it could be concluded that the coatings in regime I are not stable. As such, the stability could be linked to the WCAs and chemical composition of the coatings: if the WCAs are low and the amide content is high (regime I), the coating is not stable. If the WCAs are high and the amide content is reduced (regime III), the coating is stable. Previous stability studies of plasma polymers also observed an altered stability as a function

of layer thickness.³⁷ Therefore, the stability for the most stable coating (50 W) has also been assessed after 1, 2, and 3 min.

Figure 5B illustrates that the coating deposited at 50 W is stable for all deposition times under study. Therefore, it could be concluded that the coating stability at this power is caused by the highly cross-linked nature of the coating. At this condition, the thickness after 5 min was also measured and was found to be equal to 376.2 ± 62.1 nm. The linear fit on thickness (t) versus deposition time (dt) yields the following equation with $R^2 > 0.99$

$$t \text{ (nm)} = 80.3 \text{ (nm/min)} \times dt \text{ (min)} - 33.0$$

This illustrates that the deposition of the coating is slower during the beginning of the process but proceeds linearly afterward. Therefore, the thickness measurements shown in Figure 5A on day 0 also illustrate that until 34 W, the deposition speed increases, indicating that the deposition process takes place in the monomer-sufficient regime. After that point, the deposition proceeds in the so-called competing regime, as the coating thickness remains unaffected as a function of discharge power. This transition in the deposition regime and coating stability shows that the deposition process at low powers does not have enough energy to induce the monomer fragmentation needed to obtain stable coatings. The increase in monomer fragmentation results in higher deposition speeds and better stability. These findings are in accordance with previous studies.^{6,23}

The obtained stability over 7 days of water incubation makes these plasma-polymerized DMAM coatings very interesting for synthesizing N- and O-containing plasma polymer coatings with a significant amount of amides. Other possibilities for this purpose are the previously mentioned low-pressure plasma polymerization of 2-oxazolines and the plasma polymerization of N-containing monomers like allylamine and cyclopropylamine, both of which lead to coatings with a considerable amide content.^{35,36,45,46} However, transposing these processes to higher pressures, which is more interesting for potential applications because of no need for expensive vacuum equipment, results in changes in the surface chemistry or coating stability. For the former precursor type, XPS measurements indicated the absence of amide groups for all different conditions at the same working pressure used in this work.³¹ For the latter precursor type, obtaining stable coatings becomes even more challenging. This is exemplified by the plasma polymerization of allylamine coatings at atmospheric pressure, where the resulting coatings show a significant thickness decrease after 7 days of water incubation at the highest reported power.³⁷ Therefore, the plasma polymerization of DMAM is an interesting alternative for the synthesis of stable N- and O-containing plasma polymer coatings with a significant amount of amides at elevated pressures. Moreover, a very reproducible deposition process can be obtained in terms of coating chemistry, as it is independent of the Yasuda parameter in regime III.

3.5. OES of DMAM Plasma. OES is used in this work to study the active plasma species formed during the polymerization process. Spectra of regimes I and III were measured and are shown in Figure 6A. All peaks in the region 690–900 nm originate from atomic Ar emissions, except the shoulder at 844.6 nm, which is attributed to elementary oxygen.⁴⁷ The presence of elementary oxygen could be assigned to the rest fractions of air in the reaction chamber. The peaks in the region 200–690 nm are displayed in the Supporting

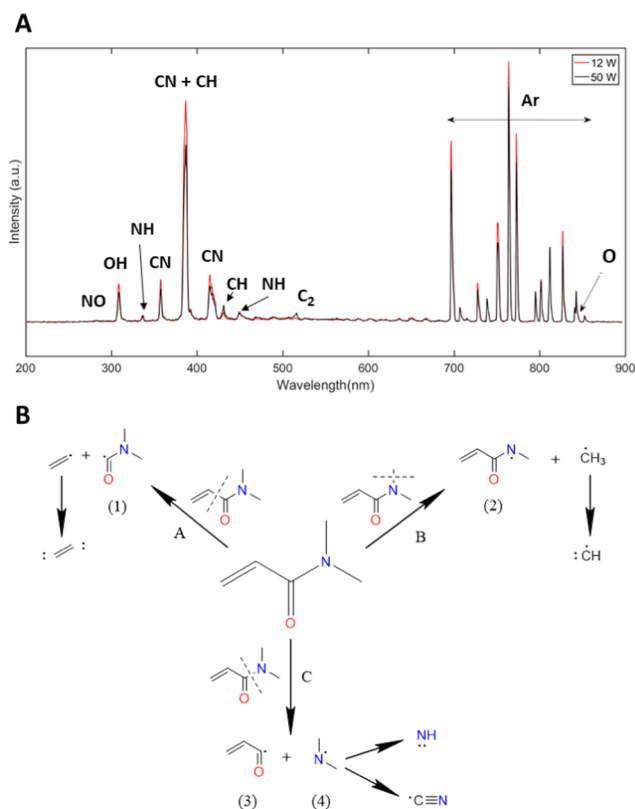


Figure 6. (A) OES spectra of the plasma gas phase sustained at 12 and 50 W. (B) Proposition of monomer fragmentation processes that lead to the observed plasma species.

Information (Table S1) for clarity reasons (obtained by using longer integration times to see the peaks more clearly). Other impurities, besides the O peak, are hydroxyl radicals (282.9, 308.9 nm), originating from water impurities in the argon gas and possibly N_2 , also due to rest fractions of air.^{48,49} The most pronounced peak of N_2 excitation is, according to the literature, the peak at 336.1 nm. However, as this peak is most likely a combination of N_2 and NH excitation, other expected peaks attributed to N_2 would be even lower. Therefore, it is expected that the peaks at 315.1, 336.1, and 357.8 nm are mostly originating from CH, NH, and CN, respectively. However, the presence of a small peak at 391.2 nm, which could be linked to N_2^+ , also made the presence of N_2 highly likely.⁴⁹ The other plasma species shown in Table 3 are due to the fragmentation of the monomer.⁵⁰

No new peaks are observed at higher powers, indicating that the increase in power does not result in new plasma fragmentation pathways. In both cases, the OES spectra are composed of the emissions of CH, NH, CN, and C_2 . Based on the presence of these species, Figure 6B shows the proposed different monomer fragmentation steps that could lead to the observed OES measurements.

The presence of C_2 suggests that the double bond could be separated from the monomer molecule as shown in fragmentation A. Hydrogen abstraction could then result in the formation of C_2 . The reactive radical on the amide carbon (product (1)) could react with other radicals in the plasma or this molecule could be further fragmented via the other proposed mechanisms B and C. The presence of CH radicals suggests that the *N*-methyl bond could be broken to form a methyl radical that can form the CH radical upon separation of H_2 . Similar to the aforementioned scission product, product (2) can either react or be further fragmented via mechanism A, B, or C. If this product reacts with hydrogen in the plasma, a secondary amide would be formed. Raman spectroscopy results show that primary amides were the least present among the amides, indicating that this fragmentation pathway is not likely to happen twice on the same monomer molecule. The presence of NH and CN radicals suggests that the amide bond was also broken, which lead to the formation of species (3) and (4). Further fragmentation of (4) and reaction with reactive hydrogen could lead to NH formation, while hydrogen abstraction at one carbon atom and further scission of the C–N bond would lead to CN formation. These fragments are also observed in OES spectra of plasma-polymerized amine-based coatings, which strengthens the validity of the proposed fragmentation mechanism.⁴⁶ The presence of CN in the plasma could be an explanation for the nitriles and *iso*-nitriles in the FTIR and Raman spectra, while the presence of NH could lead to amine incorporation in the coating. The formation of product (4) can also lead to the deposition of amines and imines. The formation of product (3) could lead to the incorporation of ketones and/or aldehydes in the coating, which was to be expected based on the comparison of C 1s and O 1s spectra. The formation of these species is in line with previously reported plasma polymerization of carbonyl-containing monomers.⁵¹ Further fragmentation of product (3) could also lead to CO species, which are expected to have a negligibly low signal in the OES spectra.⁵⁰ The low reactivity of these species, in comparison with the formed N-containing species, could be an explanation for the lower O content in comparison with the N content in the coating.⁵² However, it

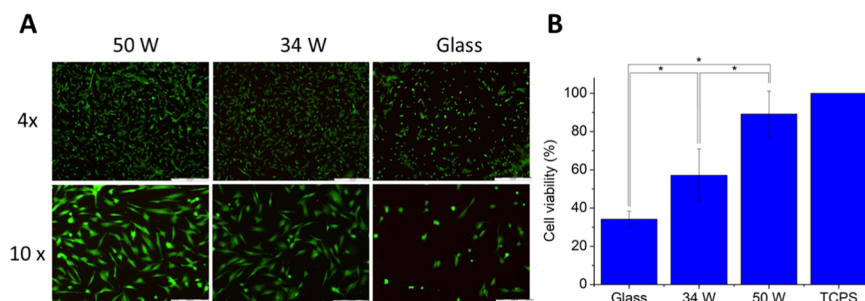


Figure 7. (A) Live/dead staining fluorescent images of cells adhering on coatings deposited at 34 and 50 W and on bare glass substrates. Scale bars are 500 and 200 μm for 4 \times and 10 \times , respectively. (B) MTS assay results for bare glass substrates, coatings deposited at 34 and 50 W, and the control TCPS. (*) Are statistically significant differences as calculated with one-way ANOVA ($p < 0.05$).

should be taken into account that the composition of a plasma polymer is determined not only by the plasma species itself but also by surface ablation of the already-deposited plasma polymer by the active plasma species. Still, the OES measurements and proposed fragmentation mechanisms seem to be in line with the chemical composition of the coating.

3.6. In Vitro Testing of Cell Adhesion on DMAM Plasma Coatings. To assess the cell-repellent/cell-adhesive properties of the stable DMAM plasma coatings, the response of MC3T3 cells to the coatings deposited at 34 and 50 W is assessed by live/dead staining. A number of representative images of the adhered cells are shown in Figure 7A. From these images, it is clear that the coatings are not cell-repellent, as a multitude of cells adhered to the coatings. A clear difference in cell morphology for the untreated and coated samples is also visible. The cells on the glass substrates had a round morphology, indicating poor cell-material interaction, while the cells on the coatings have an elongated spread-out shape, indicating good biointeractive properties of the plasma-polymerized coating. To evaluate the cytotoxicity of the coating, the cell viability is also assessed by an MTS assay 1 day after cell seeding. The results for the bare glass substrate, the two types of coating, and the reference sample (TCPS) are given in Figure 7B. Both coatings show a significantly higher cell viability than the bare glass, while the coating at 34 W ($57 \pm 14\%$) also has a significantly lower cell viability than the coating at 50 W ($89 \pm 12\%$) (one-way ANOVA, $p < 0.05$). This could be caused by the lower coating stability at 34 W, in which the coating loses a part of its thickness. Either this can negatively affect the adhesion of the cells on the coating surface, which would lead to a lower MTS signal, or the dissolved coating could be toxic, leading to lower cell viability. Additionally, trapped NO radicals could be present in the coating, as these were observed in the OES spectra of the DMAM plasma. These radicals could leach out of the coating and thereby influence the cell viability.⁵³ Most importantly, these results show that the plasma polymer does not have antifouling properties as observed for coatings of tertiary amide-based polymers. This can be caused by the formation of cell-reactive chemical groups due to the plasma fragmentation of the monomer, like amines and alcohols, at the expense of the antifouling tertiary amide groups.¹⁹ Another factor that should be taken into account is the wettability of the coating, which is probably too low for the plasma coating to possess antifouling behavior, as antifouling coatings are typically very hydrophilic and well-hydrated. For comparison, antifouling coatings that are considered to have moderate wettability show receding and advancing WCA of, respectively, 21 and 40°, which is still considerably lower than the WCA of the coatings in this work.⁵⁴ Nonetheless, coatings that induce good cell adhesion and proliferation can be interesting for scaffold modification in tissue engineering purposes, as this is a one-step process and does not require any addition of molecules as opposed to other techniques.⁵⁵

4. CONCLUSIONS

In this work, the near-atmospheric pressure plasma polymerization of *N,N*-dimethylacrylamide was studied to form coatings on glass. By utilizing multiple analysis techniques, three different regimes could be identified in the deposition process. At low powers (regime I), the coatings were not stable despite the fact that the fragmentation of the monomer was

already significant. In this regime, the coatings contained the highest amide content and were very hydrophilic. At intermediate powers (regime II), characteristics of both regimes I and III were observed, indicating a sudden transition point for the power between both regimes. At high powers (regime III), the coatings were stable, which was in agreement with the higher monomer fragmentation observed. The fragmentation process resulted in the formation of coatings with a complex chemistry, including amides, alcohols, amines, imines, unsaturated hydrocarbon bonds, nitriles, isonitriles, and ketones and/or aldehydes. The coating composition could be linked to the observed plasma species with OES. XPS depth profiling indicated a difference between the top layer and the bulk of the coating, which had a homogeneous chemical composition. The stable coatings were also tested for their cell interactions. Live/dead staining indicated good cell adhesion and survival on the coatings, and an MTS assay showed that the coatings were not toxic. This cell-interactive behavior could be linked to the cell-interactive groups in the coating and the moderate wettability of the coating. This study indicates that plasma-polymerized *N,N*-dimethylacrylamide coatings can have potential for tissue engineering purposes because of good cell viability due to extensive fragmentation of the monomer structure. Therefore, further studies can focus on the deposition of these coatings on tissue engineering scaffolds. Another possible extension of this research can be the optimization of the plasma process to deposit antifouling coatings if the monomer structure can be preserved.

■ ASSOCIATED CONTENT

Supporting Information

The Supporting Information is available free of charge at <https://pubs.acs.org/doi/10.1021/acsami.9b19526>.

Analysis of the reference polymer synthesis; chemical analysis of the reference polymers; electrical characterization of the plasma setup; ¹H NMR spectra of dissolved coatings (PDF)

■ AUTHOR INFORMATION

Corresponding Authors

*E-mail: richard.hoogenboom@ugent.be (R.H.).

*E-mail: nathalie.degeyter@ugent.be (N.D.G.).

ORCID

Pieter Cools: 0000-0003-1649-284X

Joachim F. R. Van Guyse: 0000-0001-5725-6531

Mahtab Asadian: 0000-0001-5624-3325

Andre G. Skirtach: 0000-0002-4468-7620

Richard Hoogenboom: 0000-0001-7398-2058

Notes

The authors declare no competing financial interest.

■ ACKNOWLEDGMENTS

Tim Egghe acknowledges the support of the Research Foundation Flanders (FWO) for a Ph.D. grant strategic basic research (3S33118, FWO18/SBB/070). The authors also acknowledge the support of the FWO for financing the Buckminster fullerene ion gun (medium-sized research infrastructure AUGE/15/04) for advanced chemical depth profiling of organic and polymer materials. Mahtab Asadian would like to thank FWO for financing her postdoctoral grant (1217820N). This work has also received funding from the

European Research Council (ERC) under the European Union's Seventh Framework Program (FP/2007–2013)/ERC Grant Agreement no. 335929 (PLASMATS). T.E. thanks Mathijs Baert for donating the PNIPAM and the SB-photonics expertise center. D.K. and A.G.S. thank BOF UGent (BAS094-18, BOF14/IOP/003).

REFERENCES

- (1) Majewski, P.; Jarvis, K.; Akhavan, B. S. Surface-Engineered Silica via Plasma Polymer Deposition. In *Highlights in Applied Mineralogy*; De Gruyter: Berlin, Boston, 2017; pp 99–112.
- (2) Hegemann, D. Plasma polymerization and its applications in textiles. *Indian J. Fibre Text. Res.* **2006**, *31*, 99–115.
- (3) Bitar, R.; Cools, P.; De Geyter, N.; Morent, R. Acrylic acid plasma polymerization for biomedical use. *Appl. Surf. Sci.* **2018**, *448*, 168–185.
- (4) De Geyter, N.; Morent, R.; Van Vlierberghe, S.; Dubruel, P.; Leys, C.; Schacht, E. Plasma polymerisation of siloxanes at atmospheric pressure. *Surf. Eng.* **2011**, *27*, 627–633.
- (5) Sawada, Y.; Ogawa, S.; Kogoma, M. Synthesis of plasma-polymerized tetraethoxysilane and hexamethyldisiloxane films prepared by atmospheric pressure glow discharge. *J. Phys. D: Appl. Phys.* **1995**, *28*, 1661–1669.
- (6) Siow, K. S.; Britcher, L.; Kumar, S.; Griesser, H. J. Plasma Methods for the Generation of Chemically Reactive Surfaces for Biomolecule Immobilization and Cell Colonization - A Review. *Plasma Processes Polym.* **2006**, *3*, 392–418.
- (7) Wu, Y. J.; Timmons, R. B.; Jen, J. S.; Molock, F. E. Non-fouling surfaces produced by gas phase pulsed plasma polymerization of an ultra low molecular weight ethylene oxide containing monomer. *Colloids Surf., B* **2000**, *18*, 235–248.
- (8) Brétagnot, F.; Lejeune, M.; Papadopoulou-Bouraoui, A.; Hasiwa, M.; Rauscher, H.; Ceccone, G.; Colpo, P.; Rossi, F. Fouling and non-fouling surfaces produced by plasma polymerization of ethylene oxide monomer. *Acta Biomater.* **2006**, *2*, 165–172.
- (9) Chan, K. V.; Onyshchenko, I.; Nikiforov, A.; Aziz, G.; Morent, R.; De Geyter, N. Plasma polymerization of cyclopropylamine with a sub-atmospheric pressure DBD. *Eur. Polym. J.* **2018**, *103*, 1–10.
- (10) Khurana, K.; Müller, F.; Jacobs, K.; Faidt, T.; Neurohr, J.-U.; Grandthyll, S.; Mücklich, F.; Canal, C.; Pau Ginebra, M. Plasma polymerized bioceramics for drug delivery: Do surface changes alter biological behaviour? *Eur. Polym. J.* **2018**, *107*, 25–33.
- (11) Cheng, X.; Canavan, H. E.; Stein, M. J.; Hull, J. R.; Kweskin, S. J.; Wagner, M. S.; Somorjai, G. A.; Castner, D. G.; Ratner, B. D. Surface Chemical and Mechanical Properties of Plasma Polymerized N-isopropylacrylamide. *Langmuir* **2005**, *21*, 7833–7841.
- (12) Chu, L.-Q.; Zou, X.-N.; Knoll, W.; Förch, R. Thermosensitive surfaces fabricated by plasma polymerization of N,N-diethylacrylamide. *Surf. Coat. Technol.* **2008**, *202*, 2047–2051.
- (13) Griesser, H. J. C.; Ronald, C.; Gengenbach, T. R.; Johnson, G.; Steele, J. G. Growth of human cells on plasma polymers: Putative role of amine and amide groups. *J. Biomater. Sci., Polym. Ed.* **1994**, *5*, 531–554.
- (14) Pan, Y. V.; Wesley, R. A.; Luginbuhl, R.; Denton, D. D.; Ratner, B. D. Plasma Polymerized N-Isopropylacrylamide: Synthesis and Characterization of a Smart Thermally Responsive Coating. *Biomacromolecules* **2001**, *2*, 32–36.
- (15) Bullett, N. A.; Talib, R. A.; Short, R. D.; McArthur, S. L.; Shard, A. G. Chemical and thermo-responsive characterisation of surfaces formed by plasma polymerisation of N-isopropyl acrylamide. *Surf. Interface Anal.* **2006**, *38*, 1109–1116.
- (16) Tauhardt, L.; Kempe, K.; Gottschaldt, M.; Schubert, U. S. Poly(2-oxazoline) functionalized surfaces: from modification to application. *Chem. Soc. Rev.* **2013**, *42*, 7998–8011.
- (17) Ward, M. A.; Georgiou, T. K. Thermoresponsive Polymers for Biomedical Applications. *Polymers* **2011**, *3*, 1215–1242.
- (18) Morgese, G.; Benetti, E. M. Surface Functionalization of Biomaterials by Poly(2-oxazoline)s. *Polym. Biomed.* **2017**, 457–485.
- (19) Pidhatika, B.; Rodenstein, M.; Chen, Y.; Rakhmatullina, E.; Mühlebach, A.; Acikgöz, C.; Textor, M.; Konradi, R. Comparative Stability Studies of Poly(2-methyl-2-oxazoline) and Poly(ethylene glycol) Brush Coatings. *Biointerphases* **2012**, *7*, 1.
- (20) Statz, A. R.; Barron, A. E.; Messersmith, P. B. Protein, cell and bacterial fouling resistance of polypeptoid-modified surfaces: effect of side-chain chemistry. *Soft Matter* **2008**, *4*, 131–139.
- (21) Liu, Q.; Singh, A.; Lalani, R.; Liu, L. Ultralow Fouling Polyacrylamide on Gold Surfaces via Surface-Initiated Atom Transfer Radical Polymerization. *Biomacromolecules* **2012**, *13*, 1086–1092.
- (22) Quirk, R. A.; Chan, W. C.; Davies, M. C.; Tandler, S. J. B.; Shakesheff, K. M. Poly(l-lysine)-GRGDS as a biomimetic surface modifier for poly(lactic acid). *Biomaterials* **2001**, *22*, 865–872.
- (23) Cools, P.; Declercq, H.; De Geyter, N.; Morent, R. A stability study of plasma polymerized acrylic acid films. *Appl. Surf. Sci.* **2018**, *432*, 214–223.
- (24) Friedrich, J. Mechanisms of Plasma Polymerization – Reviewed from a Chemical Point of View. *Plasma Processes Polym.* **2011**, *8*, 783–802.
- (25) Morgese, G.; Verbraeken, B.; Ramakrishna, S. N.; Gombert, Y.; Cavalli, E.; Rosenboom, J.-G.; Zenobi-Wong, M.; Spencer, N. D.; Hoogenboom, R.; Benetti, E. M. Chemical Design of Non-Ionic Polymer Brushes as Biointerfaces: Poly(2-oxazine)s Outperform Both Poly(2-oxazoline)s and PEG. *Angew. Chem., Int. Ed.* **2018**, *57*, 11667–11672.
- (26) Lerouge, S.; Barrette, J.; Ruiz, J.-C.; Sbai, M.; Savoji, H.; Saoudi, B.; Gauthier, M.; Wertheimer, M. R. Nitrogen-Rich Plasma Polymer Coatings for Biomedical Applications: Stability, Mechanical Properties and Adhesion Under Dry and Wet Conditions. *Plasma Processes Polym.* **2015**, *12*, 882–895.
- (27) Shi, F. F. Recent advances in polymer thin films prepared by plasma polymerization Synthesis, structural characterization, properties and applications. *Surf. Coat. Technol.* **1996**, *82*, 1–15.
- (28) Lin, S.-Y.; Li, M.-J.; Cheng, W.-T. FT-IR and Raman vibrational microspectroscopies used for spectral biodiagnosis of human tissues. *Spectroscopy* **2007**, *21*, 1–30.
- (29) Lai, B. F. L.; Creagh, A. L.; Janzen, J.; Haynes, C. A.; Brooks, D. E.; Kizhakkedathu, J. N. The induction of thrombus generation on nanostructured neutral polymer brush surfaces. *Biomaterials* **2010**, *31*, 6710–6718.
- (30) Divandari, M.; Morgese, G.; Ramakrishna, S. N.; Benetti, E. M. Surface-grafted assemblies of cyclic polymers: Shifting between high friction and extreme lubricity. *Eur. Polym. J.* **2019**, *110*, 301–306.
- (31) Van Guyse, J. F. R.; Cools, P.; Egghe, T.; Asadian, M.; Vergaelen, M.; Rigole, P.; Yan, W.; Benetti, E. M.; Jerca, V.-V.; Declercq, H.; Coenye, T.; Morent, R.; Hoogenboom, R.; De Geyter, N. Influence of the Aliphatic Side Chain on the Near Atmospheric Pressure Plasma Polymerization of 2-Alkyl-2-oxazolines for Biomedical Applications. *ACS Appl. Mater. Interfaces* **2019**, *11*, 31356–31366.
- (32) López, G. P.; Castner, D. G.; Ratner, B. D. XPS O 1s binding energies for polymers containing hydroxyl, ether, ketone and ester groups. *Surf. Interface Anal.* **1991**, *17*, 267–272.
- (33) Jagst, E. *Surface Functional Group Characterization Using Chemical Derivatization X-ray Photoelectron Spectroscopy (CD-XPS)* Berlin, 2011.
- (34) Bartnikas, R. Note on discharges in helium under a.c. conditions. *J. Phys. D: Appl. Phys.* **1968**, *1*, 659–661.
- (35) Bhatt, S.; Pulpytel, J.; Mirshahi, M.; Arefi-Khonsari, F. Cell Resistant Peptidomimetic Poly(2-ethyl-2-oxazoline) Coatings Developed by Low Pressure Inductively Excited Pulsed Plasma Polymerization for Biomedical Purpose. *Plasma Process. Polym.* **2015**, *12*, 519–532.
- (36) Ramiasa, M. N.; Cavallaro, A. A.; Mierczynska, A.; Christo, S. N.; Gleadle, J. M.; Hayball, J. D.; Vasilev, K. Plasma polymerised polyoxazoline thin films for biomedical applications. *Chem. Commun.* **2015**, *51*, 4279–4282.
- (37) Aziz, G.; Thukkaram, M.; De Geyter, N.; Morent, R. Plasma parameters effects on the properties, aging and stability behaviors of

allylamine plasma coated ultra-high molecular weight polyethylene (UHMWPE) films. *Appl. Surf. Sci.* **2017**, *409*, 381–395.

(38) De Geyter, N.; Morent, R.; Dubruel, P.; Leys, C. In *Plasma Polymerization of Acrylic Acid at Medium Pressure*, European Conference on Nano Films, Liège, 2010.

(39) Jafari, R.; Tatoulian, M.; Morscheidt, W.; Arefi-Khonsari, F. Stable plasma polymerized acrylic acid coating deposited on polyethylene (PE) films in a low frequency discharge (70kHz). *React. Funct. Polym.* **2006**, *66*, 1757–1765.

(40) Socrates, G. *Infrared and Raman Characteristic Group Frequencies: Tables and Charts*; John Wiley & Sons Ltd, 2001; Vol. 3.

(41) Sanz, B.; von Bilderling, C.; Tuninetti, J. S.; Pietrasanta, L.; Mijangos, C.; Longo, G. S.; Azzaroni, O.; Giussi, J. M. Thermally-induced softening of PNIPAm-based nanopillar arrays. *Soft Matter* **2017**, *13*, 2453–2464.

(42) Lin-Vien, D.; Colthup, N. B.; Fateley, W. G.; Grasselli, J. G. Compounds Containing –NH₂, –NHR, and –NR₂ Groups. In *The Handbook of Infrared and Raman Characteristic Frequencies of Organic Molecules*; Elsevier, 1991.

(43) Macgregor-Ramiasa, M. N.; Cavallaro, A. A.; Vasilev, K. Properties and reactivity of polyoxazoline plasma polymer films. *J. Mater. Chem. B* **2015**, *3*, 6327–6337.

(44) Desmet, T.; Morent, R.; De Geyter, N.; Leys, C.; Schacht, E.; Dubruel, P. Nonthermal Plasma Technology as a Versatile Strategy for Polymeric Biomaterials Surface Modification: A Review. *Biomacromolecules* **2009**, *10*, 2351–2378.

(45) Finke, B.; Luethen, F.; Schroeder, K.; Mueller, P. D.; Bergemann, C.; Frant, M.; Ohl, A.; Nebe, B. J. The effect of positively charged plasma polymerization on initial osteoblastic focal adhesion on titanium surfaces. *Biomaterials* **2007**, *28*, 4521–4534.

(46) Manakhov, A.; Zajíčková, L.; Eliáš, M.; Cechal, J.; Polčák, J.; Hnilica, J.; Bittnerová, S.; Necas, D. Optimization of Cyclopropylamine Plasma Polymerization toward Enhanced Layer Stability in Contact with Water. *Plasma Processes Polym.* **2014**, *11*, 532–544.

(47) Niksa, K.; Uros, C.; Alenka, V.; Slobodan, M.; Miran, M. An Optical-Emission-Spectroscopy characterization of oxygen plasma during the oxidation of aluminium foils. *Mater. Technol.* **2009**, *43*, 245–249.

(48) Hong, Y. J.; Nam, C. J.; Song, K. B.; Cho, G. S.; Uhm, H. S.; Choi, D. I.; Choi, E. H. Measurement of hydroxyl radical density generated from the atmospheric pressure bioplasma jet. *J. Instrum.* **2012**, *7*, No. C03046.

(49) Kim, M.; Kim, M. G.; Kim, S. R.; Chung, H. Y.; Choi, J. G.; Joh, H. M.; Chung, T. H.; Kim, H. S.; Kim, Y. Effective surface modification of a germanium layer by using an atmospheric pressure plasma jet with a round ended nozzle. *J. Korean Phys. Soc.* **2013**, *63*, 996–1000.

(50) Pearse, R. W. B.; Gaydon, A. G. *The Identification of Molecular Spectra*, 2 ed.; Chapman & Hall: London, 1950.

(51) Chilkoti, A.; Ratner, B. D.; Briggs, D. Plasma-deposited polymeric films prepared from carbonyl-containing volatile precursors: XPS chemical derivatization and static SIMS surface characterization. *Chem. Mater.* **1991**, *3*, 51–61.

(52) Chatani, N.; Murai, S.; Fukuyama, T.; Ryu, I. Carbon Monoxide. *Encycl. Reagents Org. Synth.* **2006**, DOI: 10.1002/047084289x.rc013.pub2.

(53) Villalobo, A. Nitric oxide and cell proliferation. *FEBS J.* **2006**, *273*, 2329–2344.

(54) Rodriguez-Emmenegger, C.; Brynda, E.; Riedel, T.; Houska, M.; Šubr, V.; Alles, A. B.; Hasan, E.; Gautrot, J. E.; Huck, W. T. S. Polymer Brushes Showing Non-Fouling in Blood Plasma Challenge the Currently Accepted Design of Protein Resistant Surfaces. *Macromol. Rapid Commun.* **2011**, *32*, 952–957.

(55) Muderrisoglu, C.; Saveleva, M.; Abalymov, A.; Van der Meeren, L.; Ivanova, A.; Atkin, V.; Parakhonskiy, B.; Skirtach, A. G. Nanostructured Biointerfaces Based on Bioceramic Calcium Carbonate/Hydrogel Coatings on Titanium with an Active Enzyme for Stimulating Osteoblasts Growth. *Adv. Mater. Interfaces* **2018**, *5*, No. 1800452.